JPE Journal of Photonics for Energy

PERSPECTIVE

Main performance metrics of thermophotovoltaic devices: analyzing the state of the art

Basile Roux,[a] Christophe Lucchesi,[b] Jean-Philippe Perez,[a] Pierre-Olivier Chapuis,[b] and Rodolphe Vaillon[a,c,*]

[a]IES, Univ Montpellier, CNRS, Montpellier, France
[b]CNRS, INSA-Lyon, CETHIL, UMR 5008, Villeurbanne, France
[c]LAAS-CNRS, Université de Toulouse, CNRS, Toulouse, France

ABSTRACT. Thermophotovoltaics (TPVs) differs from solar photovoltaics (PV) because pairwise efficiency and electrical power cannot be optimized simultaneously, as a consequence of spectral selectivity or photon recycling. A review of around thirty experiments conducted so far is carried out, and the achieved performances are compared with those obtained in the detailed balance limit. The link between optimal cell bandgap and emitter temperature is highlighted as a function of out-of-band radiation exchange between the emitter and the cell. The analysis reveals that almost all the experimental data reported are far from power-maximizing conditions and more focused on optimizing efficiency. At high temperature, thermal management is obviously an issue and optimizing efficiency is required to minimize heat generation. In general, it is argued that in addition to pairwise efficiency and electrical power density, heat power density is a third metric that should be considered in the design of TPV devices.

 [DOI: 10.1117/1.JPE.14.042403]

Keywords: thermophotovoltaics; detailed balance limit; spectral management; efficiency; power; heat

Paper 23057SS received Dec. 5, 2023; revised Jan. 23, 2024; accepted Jan. 30, 2024; published Feb. 28, 2024.

1 Introduction

Thermophotovoltaics (TPV), similar to solar photovoltaics (PV), refers to a method for converting thermal radiation into electricity via the photovoltaic effect. This research thematic has recently regained interest from the scientific community,[1–3] motivated by applications in waste heat recovery[4] and low-cost thermal energy storage at high temperature (TPV batteries).[5,6]

In solar PV, research is dedicated to maximizing conversion efficiency of the incident solar radiation power. This is equivalent to maximizing electrical power output. In TPV, the incident solar spectrum is replaced by that from a hot (700°C–2500°C) emitter. In addition, two main performance metrics have to be considered, which are the generated electrical power density p_{out} (W/cm^2) and the pairwise efficiency η_{pair} (%). This key quantity is defined as the ratio of p_{out} to the net radiation power density absorbed by the cell q_{abs}

$$\eta_{\text{pair}} = \frac{p_{\text{out}}}{q_{\text{abs}}}. \tag{1}$$

This equation applies regardless of the value of the view factor, in contrast to other definitions of efficiency (subsystem efficiency and full system efficiency, considering in addition losses in

*Address all correspondence to Rodolphe Vaillon, rodolphe.vaillon@cnrs.fr

the cavity between the emitter and the cell, and losses accompanying the conversion of primary energy into thermal energy,[1] respectively). In the case of a plane-parallel emitter-cell configuration (unity view factor), the pairwise efficiency is expressed as

$$\eta_{\text{pair}} = \frac{p_{\text{out}}}{\int_0^{+\infty} \varepsilon_{\text{eff}}(E) \cdot E \cdot b(E) \cdot \mathrm{d}E}. \tag{2}$$

The definitions and notations are similar to those used in Ref. 1. E is the photon energy, $b(E)$ is the hemispherical spectral photon flux density of a blackbody. ε_{eff} describes the radiative interaction between the emitter and the cell (i.e., multi-reflection in the cavity separating the emitter and the cell), and can be seen as an effective hemispherical emittance/absorptance of the emitter-cell pair

$$\varepsilon_{\text{eff}}(E) = \frac{\varepsilon_e(E)\varepsilon_c(E)}{1-(1-\varepsilon_e(E))(1-\varepsilon_c(E))}, \tag{3}$$

where ε_e and ε_c are the hemispherical emittance of the emitter and the cell, respectively. In what follows, the theoretical calculations are carried out within this framework, assuming a unity view factor.

In TPV conversion, spectral selectivity is a way to maximize the two main metrics (Fig. 1). On one hand, it consists of maximizing radiation transfer between the emitter and the cell ($\varepsilon_{\text{eff.IB}}$) for the in-band photons (i.e., having an energy $E > E_g$, the bandgap of the cell). This is achieved by maximizing emission from the hot emitter ($\varepsilon_{e.\text{IB}}$) and absorption by the cell ($\varepsilon_{c.\text{IB}}$). By doing so, electrical power generation (p_{out}) is increased, without having much impact on efficiency (η_{pair}). On the other hand, it also consists of minimizing radiation transfer between the emitter and the cell ($\varepsilon_{\text{eff.OOB}}$) for the out-of-band photons (i.e., having an energy $E < E_g$). This is realized by minimizing emission from the hot body ($\varepsilon_{e.\text{OOB}}$) or absorption by the cell ($\varepsilon_{c.\text{OOB}}$) (Fig. 1). Efficiency is greatly improved, without any impact on electrical power production. In practice, photonic engineering makes it possible to design spectrally selective emitters[7] and cells.[8]

As in Ref. 2, Fig. 2(a) clearly shows that efficiency and power output are not maximized simultaneously when spectral selectivity is applied. The theoretical values of p_{out} and η_{pair} are displayed as a function of cell bandgap (E_g) for a TPV device composed of a blackbody emitter ($\varepsilon_e = 1$) at $T_e = 1500$°C and an ideal one-stage (i.e., single-junction) cell operating at 27°C (≈300 K) in the conditions of the detailed balance limit.[9] The detailed balance theory is applied assuming the Shockley–Queisser limit[10] for the cell: absorption of in-band-photons is perfect

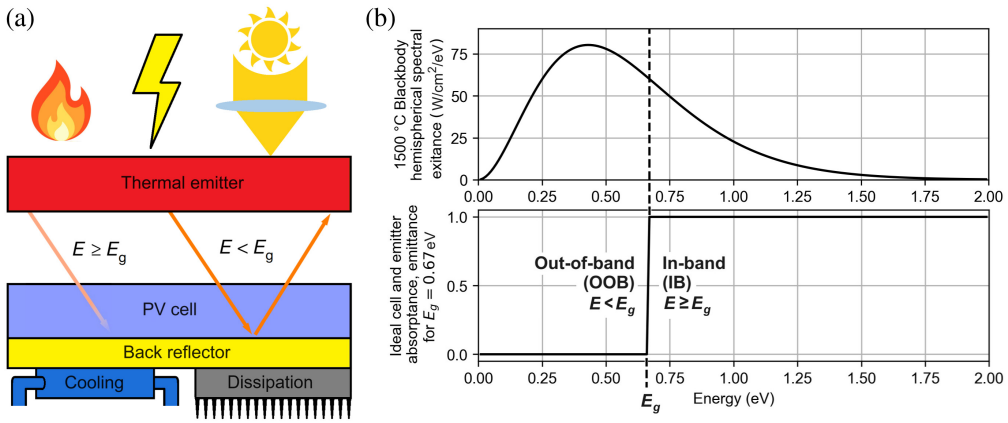

Fig. 1 Schematic representation of a TPV device composed of a thermal radiation emitter and a PV cell (a), and main quantities governing the spectral management of radiation exchange between the emitter and the PV cell (b). In the configuration shown on the schematic, ideally all in-band photons should be absorbed by the cell [$\varepsilon_c(E > E_g) = 1$], where E_g is the bandgap of a 1-stage cell], and all out-of-band photons should be reflected back to the emitter [$\varepsilon_c(E < E_g) = 0$]. Alternatively, spectral selectivity could be applied on the emitter side (ε_e). Instead of considering a blackbody emitter, $\varepsilon_e(E < E_g)$ could be minimized while $\varepsilon_e(E > E_g)$ could be maximized. By definition, the effective emittance ε_{eff} includes both possibilities.

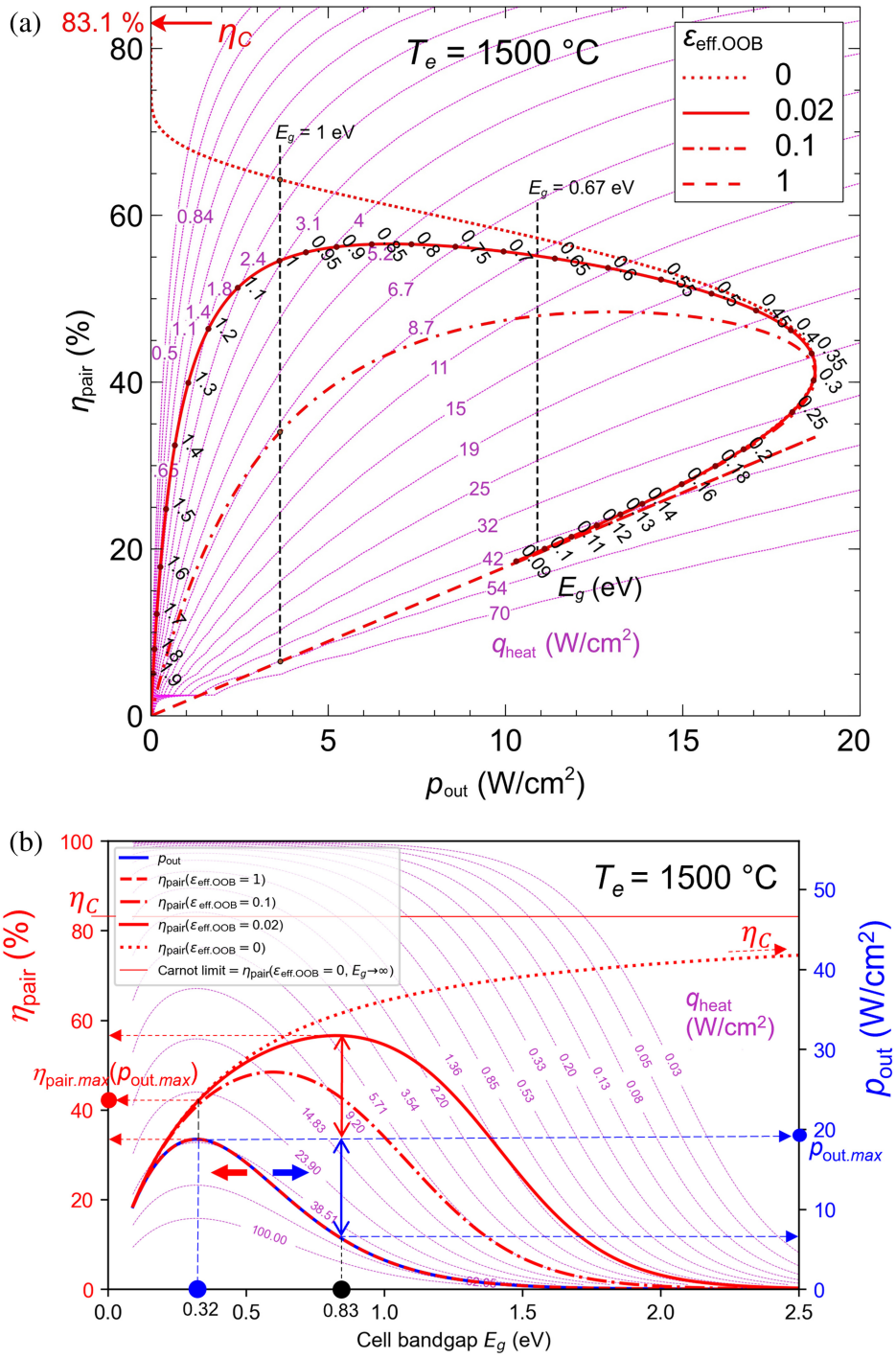

Fig. 2 Detailed balance limit calculation of pairwise efficiency and electrical power density for a TPV device composed of an emitter at 1500°C and an ideal 1-stage PV cell operating at 27°C, for selected values of the out-of-band emittance of the emitter-cell pair ($\varepsilon_{\text{eff.OOB}}$). (a) Pairwise efficiency as a function of electrical power density. (b) Pairwise efficiency and electrical power density as a function of cell bandgap. In each case, the heat power density generated in the cell, defined by Eqs. (4) and (5), is superimposed. In (b), q_{heat} must be read along the η_{pair} curve, and not the p_{out} one. η_C stands for the Carnot efficiency, equal to 83.1% at this emitter temperature.

($\varepsilon_{c.\text{IB}} = 1$), one photon generates one electron-hole pair, mobility of electron and holes is infinite, and only radiative recombination takes place.

The red dashed, dashed-dotted, solid, and dotted curves are results for different values of the out-of-band effective emittance ($\varepsilon_{\text{eff.OOB}}$, respectively 1, 0.1, 0.02, and 0, which in the present

case of a blackbody emitter is equal to the emittance of the cell ε_c). $\varepsilon_{c.\mathrm{OOB}} = 1$ (dashed red curve) means that all sub-bandgap photons are absorbed by the cell, while $\varepsilon_{c.\mathrm{OOB}} = 0$ (dotted red curve) means that all of them are reflected back to the emitter and recycled. Each point on a (p_{out}, η_{pair}) curve corresponds to a specific cell bandgap E_g. For the purpose of clarity, values of bandgap are displayed only in one case ($\varepsilon_{\mathrm{eff.OOB}} = 0.02$). As previously explained, for a given bandgap, $\varepsilon_{c.\mathrm{OOB}}$ does not have any impact on the electrical power density p_{out} while η_{pair} changes. This means that vertical lines can be drawn from the curve showing bandgap values to find them on curves for another effective OOB emittance (see the black dashed line shown for $E_g = 0.67$ and 1 eV).

Though the detailed balance limit is considered, Fig. 2(a) contains a great deal of information, valuable in less ideal configurations. First, without any spectral selectivity – i.e., out-of-band photon recycling – ($\varepsilon_{c.\mathrm{OOB}} = 1$), efficiency and electrical power are maximized at the same bandgap value (0.32 eV, see the dashed line with slope equal to $10^4/(\sigma T_e^4)$, where σ is the Stefan–Boltzmann constant). This configuration is equivalent to solar PV. However, when photon recycling is applied ($\varepsilon_{c.\mathrm{OOB}} < 1$), the optima in p_{out} and η_{pair} become distinct. In the case where out-of-band emittance of the cell is 0.02 (solid red curve), as expected maximum power output takes place at the same bandgap as before (0.32 eV), while efficiency is maximum at a bandgap of 0.83 eV. Compared to the case without any recycling (33.4%), efficiency at the maximum efficiency point is largely enhanced (56.6%), but at the expense of power output (6.7 instead of 18.7 W/cm^2 at power optimum). In the limiting case where $\varepsilon_{c.\mathrm{OOB}} \to 0$, η_{pair} tends to its maximum (83.1%) when $E_g \to \infty$, while $p_{\mathrm{out}} \to 0$. In this Shockley–Queisser analysis at zero power with no out-of-band cell absorption, the limit is given by Carnot efficiency and not the Landsberg one (see Ref. 11 for an in-depth analysis of the thermodynamic limits of radiative engines).

The same results are depicted in Fig. 2(b), where pairwise efficiency (scale on the left y-axis) and electrical power density (scale on the right y-axis) curves are plotted as a function of cell bandgap. There is only one curve for electrical power since this quantity does not depend on the out-of-band effective emittance. The scales of the two y-axes are such that the efficiency and power curves are superimposed in the case without any spectral selectivity ($\varepsilon_{\mathrm{eff.OOB}} = 1$). The observations made for Fig. 2(a) can be repeated. First, maximum power output ($p_{\mathrm{out.\,max}}$) is achieved with a cell bandgap of 0.32 eV (blue point). The split of efficiency and power curves is clearly visible as soon as the out-of-band effective emittance is smaller than 1. In the case where $\varepsilon_{\mathrm{eff.OOB}} = 0.02$ (red solid line), a gain in efficiency is possible (vertical red solid line with arrows), at the expense of a loss in power output (vertical blue solid line with arrows), with a cell bandgap of 0.83 eV (black point).

Interestingly, Fig. 2(b) exhibits clearly that with a cell bandgap ($E_g = 0.32$ eV) maximizing power output, decreasing out-of-band net radiation exchange improves efficiency, from 33.4% (when $\varepsilon_{\mathrm{eff.OOB}} = 1$) up to a maximum value ($\eta_{\mathrm{pair.\,max}}(p_{\mathrm{out.\,max}})$, red point) equal to 41.8% (when $\varepsilon_{\mathrm{eff.OOB}} = 0$). To get close to this maximum pairwise efficiency at maximum power density, it is remarkable to note that perfect spectral selectivity is not required (between $\varepsilon_{\mathrm{eff.OOB}} = 0.1$ and $\varepsilon_{\mathrm{eff.OOB}} = 0$, the gain in efficiency is only 1% absolute). This analysis of Figs. 2(a) and 2(b) illustrates that maximizing efficiency and power output cannot be pursued simultaneously: a trade-off must be found.

An additional quantity, often overlooked, has to be taken into account: the heat power density generated in the cell (q_{heat}). Having in mind that the net heat radiation power absorbed by the cell (q_{abs}) is either converted into electrical power or into thermal power

$$q_{\mathrm{abs}} = p_{\mathrm{out}} + q_{\mathrm{heat}}, \tag{4}$$

heat power density generated in the cell is unambiguously calculated from the two main metrics

$$q_{\mathrm{heat}} = p_{\mathrm{out}}\left(\frac{1}{\eta_{\mathrm{pair}}} - 1\right). \tag{5}$$

Isolines (purple dotted lines) for selected values of the generated heat power density (W/cm^2) are added to Figs. 2(a) and 2(b). Proportionality to electrical power and to the inverse of efficiency are clearly visible. Of course, reflecting out the out-of-band photons is also reducing

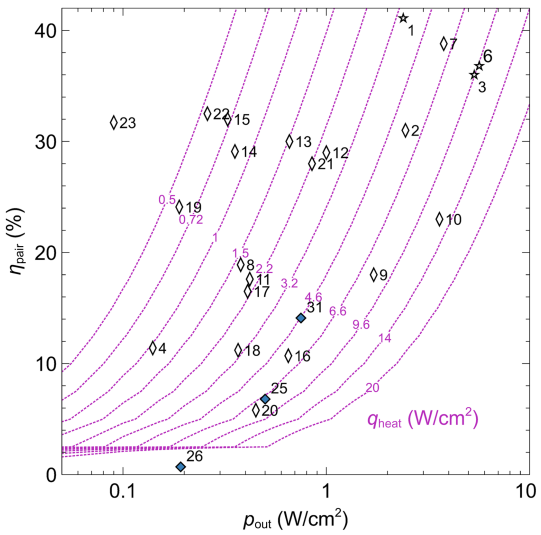

Fig. 3 Main performance metrics of the TPV experiments listed in Table 1 (first column numbers). Stars are for devices with a multijunction cell, white diamonds for far-field TPV devices, and blue diamonds for near-field TPV devices.

the heat generated in the cell together with an enhancement of efficiency. In addition to the analysis of the evolution of the heat source with the main metrics, it seems even more important to stress out the level of heat that needs to be dissipated to the environment to keep the cell at room temperature. Even at the point of maximum efficiency with 98% of OOB reflected photons, 5.1 W/cm^2 have to be evacuated to keep the cell at 27°C. This requirement of large heat flux dissipation, and its consequences, are commented later. It goes without saying that this situation worsens at higher emitter temperatures.

Experimental data from the literature on the main performance metrics are shown in Fig. 3. Information about each data point is provided in Table 1. Though the detailed balance limit cannot be calculated in the near field, data are shown. No clear trend can be extracted from the cloud of data-points. It is important to have in mind that this representation of main performance metrics (p_{out}, η_{pair}, plus q_{heat}) does not depict the effects of emitter temperature and cell bandgap. There are very few cases where the electrical power density is larger than 1 W/cm^2. Four of these cases are with efficiency above 30%, leading to a generated heat density comprised between 3 and 12 W/cm^2. The dual-junction (also named tandem) cells have the best performances, both in terms of power output and efficiency. Some cases with very low efficiency (not shown) generate an enormous amount of heat.

The purpose of the following is to analyze in more details these experimental data, with respect to the detailed balance limit, as a function of emitter temperature T_e and cell bandgap E_g. The next three sections deal with a separate analysis in p_{out}, then in η_{pair}, and finally in q_{heat}.

2 Analysis in p_{out}

The parameter primarily affecting the power output density is the emitter temperature. According to the Stefan-Boltzmann law, in the case of a blackbody emitter, radiation power incident on the cell increases monotonically in proportion to the fourth power of emitter temperature (T_e). Considering a given emitter temperature but a variable cell bandgap, several losses take place in the detailed balance limit. Power output is limited by current (photogeneration) when the bandgap tends to infinity, and by voltage (radiative recombination) when the bandgap tends to zero. The first loss, due to the OOB photons (with $E < E_g$) which cannot contribute to generating electrical power, is also referring to the so-called sub-bandgap loss. An additional loss contributes for photon energies at the other side of the bandgap. Called thermalization loss, it takes place for the in-band (IB) photons (with $E > E_g$), and is caused by conversion into heat of photon energy exceeding E_g. Competition of these losses leads to the existence of an optimum cell bandgap maximizing electrical power for a given emitter temperature.

Table 1 List of TPV experiments considered in the analysis and main parameters. E_g is the cell bandgap(s), T_e the emitter temperature, T_c the cell temperature, η_{pair} the pairwise efficiency, p_{out} the electrical power density, q_{heat} the heat power density generated in the cell (calculated from η_{pair} and p_{out}). Data related to OOB spectral management must be considered with caution as only mean values of OOB emittance (either normal or hemispherical) are provided here. Most works focus on the radiative properties of either the cell ε_c or the emitter ε_e, and thus ε_{eff} cannot be properly determined. ND means "No Data." The numbers in the first column (not the reference numbers) are used in the figures.

n°	References	E_g (eV)	T_e (°C)	T_c (°C)	η_{pair} (%)	p_{out} (W/cm^2)	q_{heat} (W/cm^2)	OOB spectral management	Cell absorbing layer(s)
1	LaPotin et al. (2022)[12,a]	1.2/1.4	2400	60	41.1	2.39	3.43	$\varepsilon_c = 0.069$	AlGaInAs / GaInAs
2	Narayan et al. (2020)[13,b]	1.42	2330	ND	31	2.45	5.45	$\varepsilon_c = 0.05$	GaAs
3	Schulte et al. (2020)[14,a]	1/1.2	2150	25	36	5.34	9.49	$\varepsilon_c = 0.086$	GaInAs / AlGaInAs
4	Chemisana et al. (2023)[15,b]	1.126	2100	25	11.4	0.14	1.09	$\varepsilon_c = 0.7$	Si
5	Swanson (1980)[16,b]	1.11	2027	ND	29	ND	ND	ND	Si
6	Tervo et al. (2022)[17,a]	0.74/0.84	1900	24	36.8	5.65	9.7	$\varepsilon_c = 0.073$	GaInAs / GaInPAs
7	Tervo et al. (2022)[17,b]	0.74	1850	24	38.8	3.78	5.96	$\varepsilon_c = 0.053$	GaInAs
8	Lee et al. (2022)[18,b]	1.11	1715	25	18.9	0.379	1.63	$\varepsilon_c = 0.02$	Si
9	Bhatt et al. (2020)[19,b]	0.72	1403	43	18	1.71	7.79	$\varepsilon_c = 0.55$	GaSb
10	Shimizu et al. (2015)[20,b]	0.67	1367	45	23	3.6	12.05	ND	GaSb
11	Kohiyama et al. (2016)[21,b]	0.67	1367	ND	17.6	0.42	1.97	ND	GaSb
12	Fraas et al. (2001)[22,b]	0.73	1275	50	29	1	2.45	ND	GaSb
13	Narayan et al. (2020)[13,b]	0.74	1300	ND	30	0.658	1.54	$\varepsilon_c = 0.047$	InGaAs
14	Omair et al. (2019)[23,b]	0.75	1207	ND	29.1	0.355	0.86	$\varepsilon_c = 0.054$	InGaAs
15	Fan et al. (2020)[8,b]	0.74	1182	20	32.03	0.327	0.69	$\varepsilon_c = 0.018$	InGaAs
16	Zhang et al. (2020)[24,b]	0.53	1197	25	10.65	0.65	5.45	ND	InGaAsSb
17	Fernandez et al. (2007)[25,b]	0.67	1100	ND	16.5	0.41	2.07	$\varepsilon_c = 0.15$	Ge

Table 1 (*Continued*).

n°	References	E_g (eV)	T_e (°C)	T_c (°C)	η_{pair} (%)	p_{out} (W/cm^2)	q_{heat} (W/cm^2)	OOB spectral management	Cell absorbing layer(s)
18	Suemitsu (2020)[26,b]	0.7	1065	10	11.2	0.368	2.92	ND	GaSb
19	Burger et al. (2022)[27,b]	0.74	1036	29	32.5	0.26	0.54	$\varepsilon_c = 0.009$	InGaAs
20	Lim et al. (2023)[28,b]	0.74	1006	20	31.7	0.09	0.19	$\varepsilon_c = 0.011$	InGaAs
21	Woolf et al. (2018)[29,b]	0.6	1055	ND	24.1	0.189	0.6	$\varepsilon_e = 0.53$	InGaAs
22	Lenert et al. (2014)[30,b]	0.55	962	20	5.8	0.45	7.3	ND	InGaAsSb
23	Dashiel et al. (2006)[31,b]	0.53	950	27	28	0.85	2.19	$\varepsilon_{eff} = 0.057$	InGaAsSb
24	Lu et al. (2018)[32,b]	0.35	800	−173	10	0.00035	0.00315	ND	InAs
25	Mittapally et al. (2021)[33,c]	0.75	997	25	6.8	0.5	6.85	ND	InGaAs
26	Inoue et al. (2021)[34,c]	0.73	919	27	0.7	0.192	27.24	ND	InGaAs
27	Inoue et al. (2019)[35,c]	0.73	792	92	0.98	$7.5\ 10^{-4}$	0.076	ND	InGaAs
28	Song et al. (2022)[36,c]	0.72	513	30	$7\ 10^{-4}$	$7.7\ 10^{-6}$	1.1	ND	GaSb
29	Bhatt et al. (2020)[37,c]	0.67	607	20	$3\ 10^{-5}$	$1.25\ 10^{-6}$	4.17	ND	Ge
30	Fiorino et al. (2018)[38,c]	0.345	382	25	0.015	$3.1\ 10^{-8}$	0.0002	ND	InAsSb
31	Lucchesi et al. (2021)[39,c]	0.23	457	−196	14.1	0.75	4.57	ND	InSb

[a]Multijunction cell.
[b]Single junction cell.
[c]Near-field TPV device.

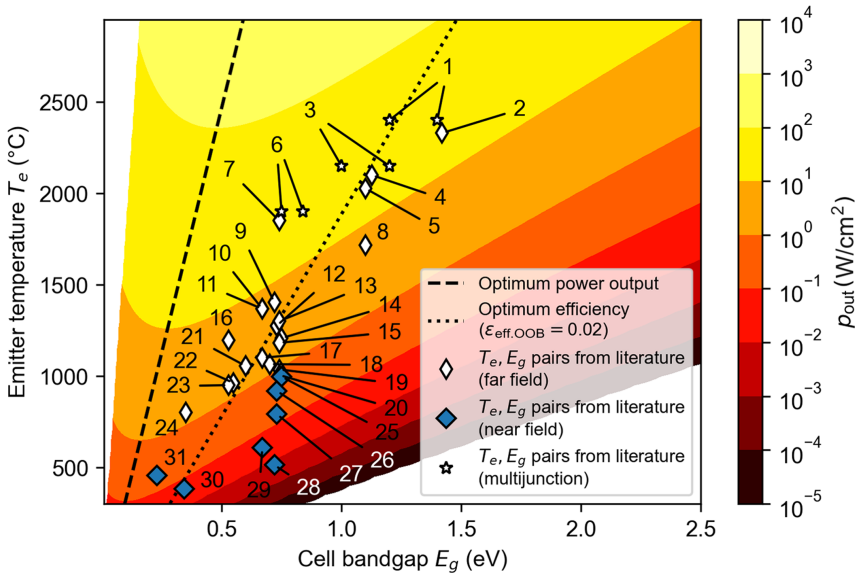

Fig. 4 Power output colormap for a TPV device in the detailed balance limit, as a function of (blackbody) emitter temperature and cell bandgap. (E_g, T_e) points from experimental data listed in Table 1 are represented (first column numbers), but their position on the colormap does not reflect the real power output, which was measured.

Figure 4 shows the power output resulting from detailed-balance limit calculations (colormap) as a function of emitter temperature (assumed to be a blackbody) and cell bandgap. It illustrates the existence of this optimum cell bandgap for electrical power generation. The maximum power output line (i.e. showing the optimum E_g as a function of T_e) is highlighted by the dashed line. It spans from $E_g = 0.15$ eV at $T_e = 300$°C to $E_g = 0.6$ eV at $T_e = 3000$°C (its approximated expression is $E_g\,(\text{eV}) = 12 \cdot 10^{-5} T_e(°\text{C}) + 0.24$, valid only above few hundreds of degrees Celsius, which differs slightly from the analytical expression suggested in Ref. 40). To be fully clear, this means that to maximize power output for an emitter temperature smaller than 3000°C, the cell bandgap has to be smaller than 0.6 eV (or the cutoff wavelength has to be larger than ≈ 2 μm).

In practice, very few experiments were conducted with cells having such low bandgaps. This path is quite a challenge, as real cells experience increasing non-radiative losses as bandgap decreases, which is not accounted for by the detailed-balance limit. Including bandgap-dependent non-radiative losses in detailed-balance calculations would probably shift the bandagp optimizing power to higher values. Points with coordinates corresponding to the cell bandgap and the emitter temperature of TPV experiments listed in Table 1 (first column numbers) are represented by symbols in Fig. 4. The white diamonds are for devices with far-field radiation exchange and one-stage (single-junction) cells. Dual stars are for far-field TPV devices involving multijunction cells (one star per bandgap of sub-cell). Blue diamonds are for near-field TPV devices, where the distance between the emitter and the PV cell is smaller than the characteristic wavelength of thermal radiation given by Wien's law (see recent reviews in Refs. 41 and 42). It is important to have in mind that power output of these devices is not that shown by the colormap. One can notice that most of the data-points are mostly shifted from the optimum power output line toward higher cell bandgaps. This indicates that so far, p_{out} does not seem to have been the main performance metric looked for. The analysis in η_{pair} and q_{heat} (closely related to p_{out}) in the following sections will shed more light on this observation.

Figure 5 shows the ratio of actual power output of the experimental data (first column numbers) to the power output given by the detailed balance limit, with the cell absorbing layer bandgap, cell temperature and emitter temperature being those used in the experiments. The main conclusion is that power output is the performance metric for which there is the largest room for improvement. Most data-points for far-field experiments are with a power output lower than

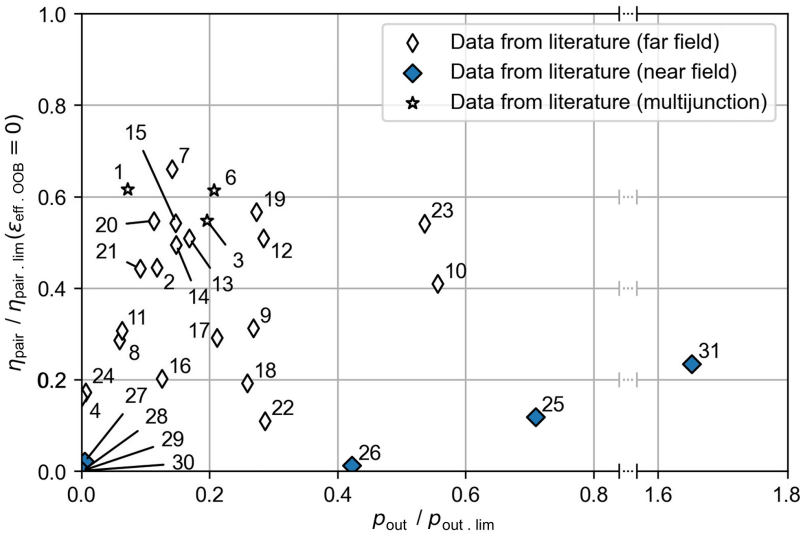

Fig. 5 Pairwise efficiency η_{pair} and power output p_{out} of the experimental data listed in Table 1 (first column numbers), normalized by the corresponding value in the detailed-balance limit $\eta_{pair.lim}$ and $p_{out.lim}$ (considering the same emitter and cell temperatures, and same cell bandgap as in the experiment). For consistency of the comparisons, $\eta_{pair.lim}$ and $p_{out.lim}$ were all computed for a one-stage cell in far-field conditions, with perfect reflection of OOB photons ($\varepsilon_{eff.OOB} = 0$). In the case of experiments with a multijunction cell, the bandgap was taken as the mean value of the sub-cell bandgaps. When no data on the cell temperature were available, calculations were made at 27°C.

one third of the limit (only two data-points are approaching 0.6). There are several possible explanations for these observations: (1) the emitter is not a blackbody in the IB spectral range; (2) a large fraction of the IB photons are reflected by the cell (an antireflecting photonic structure is missing or not efficient enough); (3) the IB photons are not fully absorbed for generating electron-hole pairs in the active layers of the cell; (4) the nonfundamental electrical losses (e.g., non-radiative recombination, Joule effect, etc.) are too large; (5) the view factor between the cell and the emitter is too low, and a lot of power radiated by the emitter is lost in the cavity. Even though data are not always available, it seems that most of the experiments performed so far were made with small view factors.[43] As for near-field TPV devices, only one of them exceeds the power output calculated in the radiative limit and in the far field.

3 Analysis in η_{pair}

Pairwise efficiency, as defined in Eq. (2), is proportional to p_{out} and thus follows a similar trend versus T_e and E_g, with the existence of an optimum cell bandgap for a given emitter temperature. The huge difference comes from the denominator which can be reduced if OOB photons are reflected back to the emitter (i.e., when $\varepsilon_{eff.OOB} < 1$). In Fig. 6, the detailed balance limit of pairwise efficiency is shown as a colormap as a function of cell bandgap and emitter temperature in the case where the out-of-band effective emittance of the cell-emitter pair is equal to 0.02 (meaning that 98% of the OOB photons are recycled toward the emitter).

The dashed line represents the loci of maximum power output, shown to illustrate once again the splitting between optimum power generation and optimum efficiency when photon recycling is taking place. The dotted line represents the combinations (E_g, T_e) maximizing pairwise efficiency with an OOB cell reflectance of 98% (effective emittance of 0.02; similar lines are shown in Appendix A for other values of the effective emittance). The points with coordinates corresponding to the cell bandgap and emitter temperature used in the TPV experiments listed in Table 1 are shown using the same symbols as in Fig. 4. Again, it is important to have in mind that the value of pairwise efficiency for each data-point is not that shown by the colormap (efficiency in the detailed balance limit, which is larger as shown in Fig. 5). The experimental

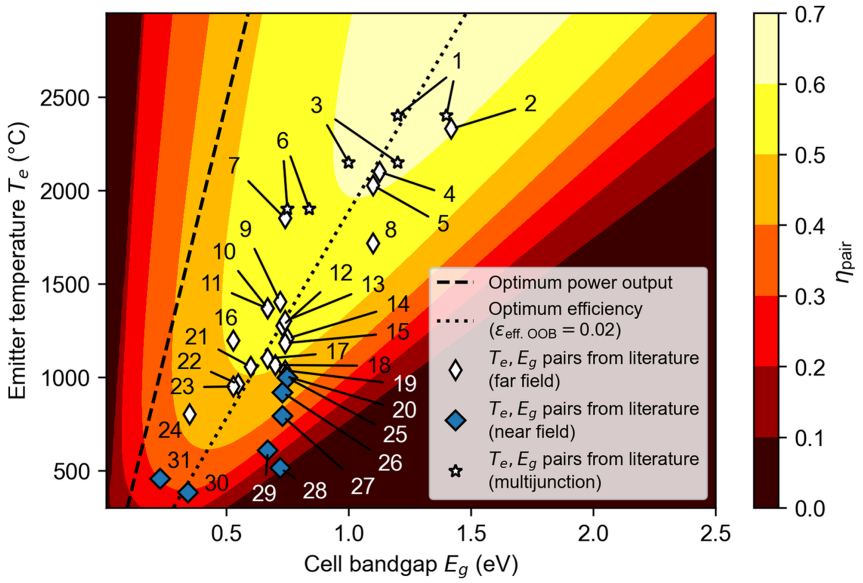

Fig. 6 Pairwise efficiency colormap for a TPV device in the detailed balance limit, as a function of (blackbody) emitter temperature and cell bandgap. (E_g, T_e) points from experimental data listed in Table 1 (first column numbers) are represented, but their position on the colormap does not reflect the real efficiency which was measured.

data-points for far-field TPV devices are way closer to this line than to the line maximizing power output. This means that these devices are intended to optimize efficiency rather than power output. Figure 5 quantitatively confirms this statement, by depicting the ratio of actual efficiency to the efficiency calculated by the detailed-balance limit in the operating conditions of the experiments. A dozen of experiments are with this ratio close to or exceeding 0.5. Halfway to optimum, it is a good score, but there is still room for improvement, even if not as much as power improvement. Suppressing out-of-band radiation exchange is the way to increase pairwise efficiency. In addition, mitigating in-band parasitic absorption (not generating electron-hole pairs) and electrical losses improves both efficiency and power output.

As for near-field TPV devices, except the two data-points with the lowest cell bandgaps (<0.5 eV) and emitter temperatures (<500°C), they were conducted with cell bandgaps which are too large for optimizing power output in the far field, even though the purpose of near-field effects is to tremendously enhance power generation. In other words, it means that the selected bandgaps were such that near-field enhancement would serve primarily to reach the power output of the best cells (having a lower bandgap) in the far field, before trying to exceed it. As already discussed, this statement is confirmed by Fig. 5, where there is only one near-field TPV device exceeding the power output of the detailed balance limit in the far field. Also, the cells used in these near-field experiments are mostly made of III-V semiconductor materials, known to lead to huge OOB absorption in the near field because of phonon polaritons, and thus to degrade efficiency.[44]

4 Analysis in q_{heat}

Often overlooked, heat power density (q_{heat}) generated in the PV cell is a third performance metric deserving to be considered. It is directly derived from power output density and pairwise efficiency as shown by Eq. (5). Figure 7 shows a colormap representation of this heat power when the pairwise efficiency is calculated in the detailed balance limit and when the OOB emittance (absorptance) of the cell is only 0.02. This case is highly favorable to reducing heat generated within the cell since 98% of OOB photons are reflected back to the (blackbody) emitter instead of being absorbed and generating heat in the cell. Despite that, it is unsurprisingly observed that heat power is tremendously increasing with emitter temperature. The points with coordinates corresponding to the cell bandgap and the emitter temperature used in the TPV

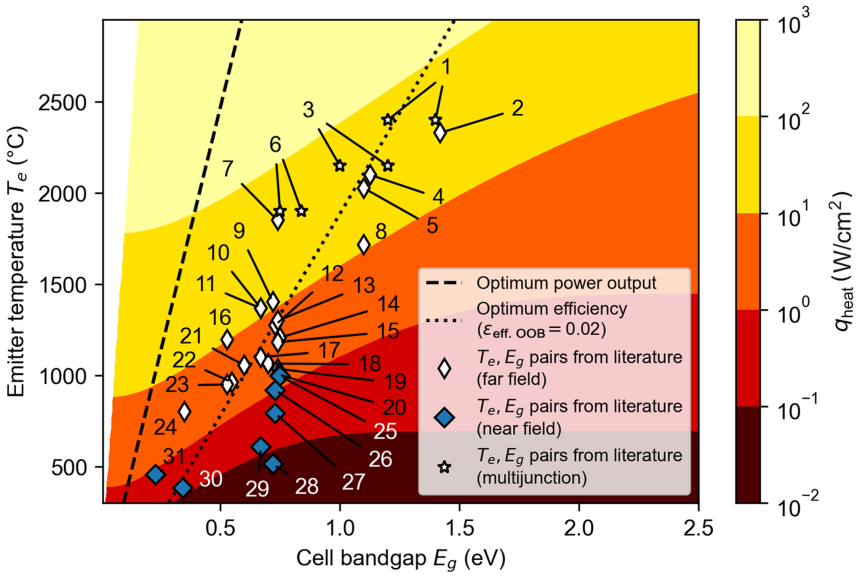

Fig. 7 Colormap of the heat generated in the cell for a TPV device in the detailed balance limit, as a function of (blackbody) emitter temperature and cell bandgap. E_g, T_e points from experimental data listed in Table 1 (first column numbers) are represented. Their position on the colormap does not reflect the real heat power density, which results from the measured power output and pairwise efficiency.

experiments listed in Table 1 are shown using the usual symbols. Again, it is important to have in mind that the actual value of heat power generated in the cell for each data-point is not that shown by the colormap.

The actual values of heat power generated in the cell of the experiments listed in Table 1 are shown in Fig. 8 as a function of power output. Proportion of this heat production in the experiments compared to that of the detailed balance limit is shown in Appendix B (Fig. 10). As expected, heat generated in the cell increases as power output rises. As shown by Eq. (5), the

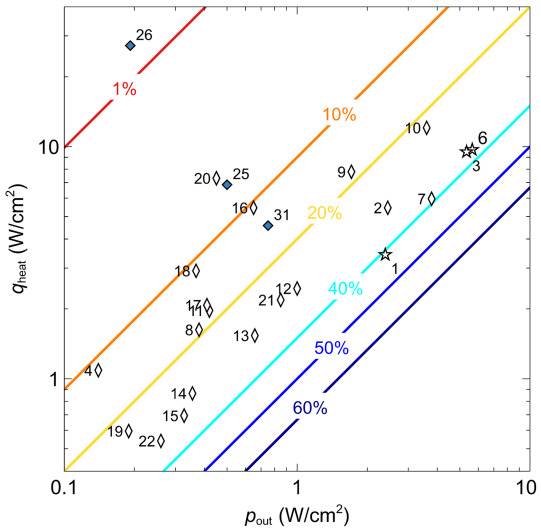

Fig. 8 Heat power density generated in the cell as a function of electrical power density, for the experimental data listed in Table 1 (first column numbers). The color lines depict the linear relation between q_{heat} and p_{out} for selected values of the pairwise efficiency (η_{pair}): 1%, 10%, 20%, 40%, 50%, and 60%. The corresponding slopes of the lines are 99, 9, 4, 1.5, 1, and 0.67, respectively. Please note that a log-log scale is used, otherwise most data points would be clustered near the left corner.

slope of linear increase in heat power with electrical power depends on the inverse of the pairwise efficiency ($q_{heat} \propto (1/\eta_{pair} - 1)$). The lines on Fig. 8 clearly indicate that efficiency must improve with power output to avoid overheating of the cell. Otherwise, heat power density may exceed that of the detailed balance limit (see Fig. 10).

For two devices with multijunction cells producing the largest power output, excessive heating is avoided thanks to a pairwise efficiency close to 40%. However, as explained previously, it is not possible to maximize simultaneously efficiency and power output. To fully understand what it means, in the case of Fig. 2 where the emitter is at 1500 °C, a low cell bandgap is required to maximize power output. If heat generated in the cell is too large to be manageable, improving efficiency means giving up some of the power produced by increasing the bandgap of the cell. This is certainly a necessity for high-temperature emitters, where heat flux levels become very large. This analysis may explain why the experimental data-points in the upper parts of Figs. 4 and 6 deviate from the optimum power line.

It is also interesting to note that among the three data-points of near-field TPV devices that fall within the axis-ranges shown in Fig. 8, significant heating occurs because of low efficiency. This observation is confirmed in Fig. 10 (Appendix B) where more data-points show overheating cases. There are various strategies to avoid an increase in cell temperature under these conditions. First, very efficient cooling systems can be used. In this case and more generally, the cooling system requires to have a much cooler body available nearby and a large thermal conductance with it to dissipate the heat. In real-life conditions, this may be difficult. A second strategy is to allow the photovoltaic cell to operate at a temperature above ambient. In this case, degradation of photovoltaic conversion performance with increasing temperature[45] has to be examined carefully.

Passive heat dissipation by conduction into a heat sink is possible, but this induces strong constraints on the size of the cell since $h \approx \lambda/R$ (the conductance from a disk to a semi-infinite medium is $4\lambda R$), where h is the heat transfer coefficient, λ the thermal conductivity of the heat sink and R the radius of the cell. As an example, for 1 W/cm^2 of heat to be dissipated (lower region of Fig. 8) in a bulky material of thermal conductivity of the order of 100 W/m.K, the cell radius R is required to be smaller than 1 cm for an allowed temperature increase of 1 K. Scalability is an issue with this strategy, as the heat sink volume should be larger than R^3.

5 Conclusion

Analysis of a set of experimental data on the performances of TPV devices has been proposed. Three fundamental metrics have been selected: pairwise efficiency (η_{pair}), electrical power density (p_{out}) and heat power density generated in the cell (q_{heat}). Since these three metrics are related to each other, it is possible to use a single graphic showing them. For selected operating temperatures of the emitter (T_e) and the cell (T_c), detailed-balance calculations in the radiative limit unambiguously show that optimum efficiency and power output cannot be achieved at the same cell bandgap when out-of-band radiation exchange between the emitter and the cell is reduced. The heat that must be dissipated to maintain the cell temperature at T_c is also a factor to be taken into account.

Separate analyses in pairwise efficiency, power output, and heat generated in the cell, using comparisons of experimental data against detailed-balance-limit calculations, have provided a great deal of information about the trends in TPV design strategies adopted until now. In particular, it appears that the cell bandgaps selected for most far-field TPV devices are tailored to achieve optimum efficiency with high spectral selectivity (ensuring that almost no out-of-band photons are absorbed by the cell) rather than to maximize output power. It seems that even in these cases, electrical power could be improved by using photonic structures ensuring maximum emission of in-band photons by the emitter, and their maximum absorption by the cell. The view factor between the emitter and the cell should also be close to one, both to maximize electrical power and to guarantee photon recycling conditions (when this strategy is chosen for spectral selectivity). Interestingly, although the purpose of near-field TPV devices is to maximize power output, many of the cells have a bandgap far from that maximizing electrical power in the far field. The analysis of heat generation in the cell has emphasized that thermal management, mostly overlooked, should be considered carefully. A current research path aims at

improving the electrical power density of TPV devices. This quest is accompanied by various challenges: on the emitter side with very high temperatures, on the cell side with very low band gaps, etc., which require advances in growth and processing techniques. But the heat to be dissipated increases proportionately, so efficiency must also be improved. However, it is not possible to optimize both simultaneously, so a clear direction has to be chosen. Making the right choice should probably take into account a complete TPV system, including the primary source of energy, and techno-economic factors. The design strategy would clearly depend on the source providing thermal energy (e.g., electrical energy for TPV batteries, solar energy, waste heat, etc.).

As a side remark, only spectral management of out-of-band photons has been considered for improving efficiency and mitigating heat generation. Similarly, spectral tailoring of the in-band photons could be useful. For instance, filtering high-energy photons could be used to mitigate the thermalization losses (and thus heat generation in the cell) and to increase efficiency, but at the expense of power output.[46,47] However, the conditions optimizing the main metrics with this strategy have yet to be thoroughly analyzed and implemented in real TPV devices.

6 Appendix A: Optimum Pairwise Efficiency Lines as a Function of the Effective Out-of-Band Emittance

For a given emitter temperature, Fig. 9 shows the deviation toward higher cell bandgap optimizing pairwise efficiency as radiation exchange between the emitter and the cell is minimized (decreasing values of the out-of-band effective emittance of emitter-cell pair). These curves can be compared to the values in Table 1 where most experiments using back reflectors display equivalent $\varepsilon_{\text{eff.OOB}}$ around 0.05. The very low OOB cell emittance ($\varepsilon_{c.\text{OOB}} = 0.009$) in Ref. 27 is explained by the use of a strategy based on a semitransparent cell. Apart from Refs. 29 and 31, emittance of the emitters is not generally taken into account in depth, leaving room for improvement on that aspect.

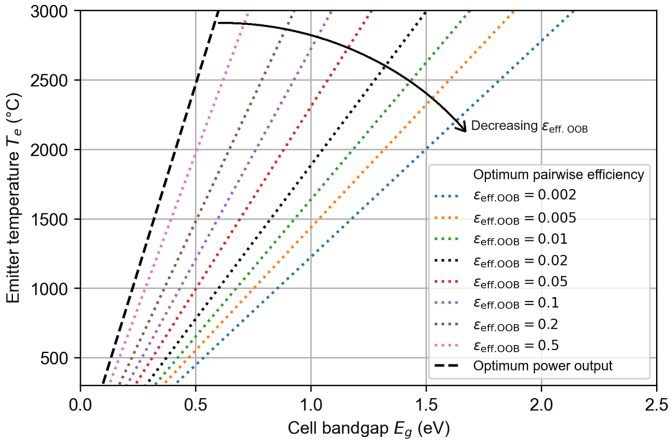

Fig. 9 Lines representing the combinations (E_g, T_e) maximizing pairwise efficiency in the detailed balance limit for various values of the out-of-band effective emittance.

7 Appendix B: Comparison of Measured Electrical Power and Resulting Heat Power Generated in the Cell With Respect to Their Value in the Detailed Balance Limit

Figure 10 illustrates that heat power generation in the cell in experiments may exceed that of the detailed balance limit, in particular when pairwise efficiency is very low. Excluding the near-field experiments, this figure somewhat illustrates the correlation existing between the quantities q_{heat} and p_{out}.

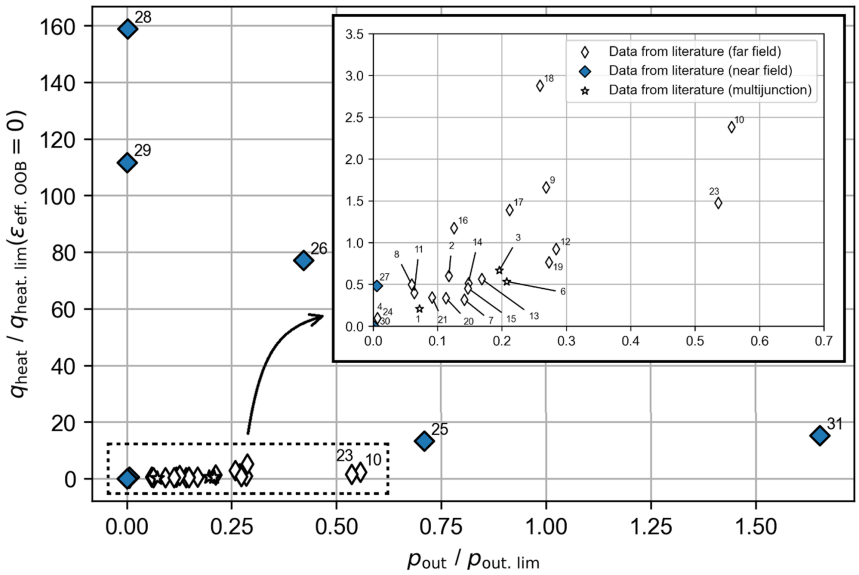

Fig. 10 Heat power density q_{heat} and power output p_{out} of the experimental data listed in Table 1 (first column numbers), normalized by the corresponding value in the detailed-balance limit $q_{heat.\,lim}$ and $p_{out.\,lim}$ (considering the same emitter and cell temperatures, and same cell bandgap as in the experiment). For consistency of the comparisons, calculations were made for a one-stage cell in far-field conditions, with perfect reflection of OOB photons ($\varepsilon_{eff.OOB} = 0$). In the case of experiments with a multijunction cell, the bandgap was taken as the mean value of the sub-cell bandgaps. When no data on the cell temperature were available, calculations were made at 27°C.

Code and Data Availability

Main data that support the findings of this study are available in Table 1 and in references cited therein. Calculations of the detailed-balance limit are elementary. Thus the code used does not need to be shared publicly, and assistance from the corresponding author is possible upon reasonable request.

Acknowledgments

Financial supports by the French National Research Agency (ANR) under grants ANR-16-CE05-0013 (DEMO-NFR-TPV) and ANR-21-CE50-0018 (LOW-GAP-TPV), by the European Commission under grant 2020-EIC-FETPROACT-2019/GA951976 (TPX-Power), and by CNRS-INSIS (project-team TREE) are acknowledged.

References

1. T. Burger et al., "Present efficiencies and future opportunities in thermophotovoltaics," *Joule* **4**(8), 1660–1680 (2020).
2. A. Datas and R. Vaillon, "Thermophotovoltaic energy conversion," in *Ultra-high Temperature Thermal Energy Storage, Transfer and Conversion*, pp. 285–308, Woodhead Publishing (2021).
3. A. Datas et al., "Advances in thermophotovoltaics: materials, devices, and systems," *Solar Energy Mater. Solar Cells* **240**, 111711 (2022).
4. S. Chen et al., "A review on current development of thermophotovoltaic technology in heat recovery," *Int. J. Extreme Manuf.* **6**, 022009 (2024).
5. C. Amy et al., "Thermal energy grid storage: liquid containment and pumping above 2000 °C," *Appl. Energy* **308**, 118081 (2022).
6. A. Datas et al., "Latent heat thermophotovoltaic batteries," *Joule* **6**(2), 418–443 (2022).
7. Z. Wang et al., "Selective emitter materials and designs for high-temperature thermophotovoltaic applications," *Solar Energy Mater. Solar Cells* **238**, 111554 (2022).
8. D. Fan et al., "Near-perfect photon utilization in an air-bridge thermophotovoltaic cell," *Nature* **586**(7828), 237–241 (2020).
9. A. Datas and C. Algora, "Detailed balance analysis of solar thermophotovoltaic systems made up of single junction photovoltaic cells and broadband thermal emitters," *Solar Energy Mater. Solar Cells* **94**(12), 2137–2147 (2010).

10. W. Shockley and H. J. Queisser, "Detailed balance limit of efficiency of p-n junction solar cells," *J. Appl. Phys.* **32**(3), 510–519 (1961).
11. M. Giteau, M. F. Picardi, and G. T. Papadakis, "Thermodynamic performance bounds for radiative heat engines," *Phys. Rev. Appl.* **20**, L061003 (2023).
12. A. LaPotin et al., "Thermophotovoltaic efficiency of 40%," *Nature* **604**(7905), 287–291 (2022).
13. T. C. Narayan et al., "World record demonstration of >30% thermophotovoltaic conversion efficiency," in *47th IEEE Photovoltaic Spec. Conf. (PVSC)*, IEEE, pp. 1792–1795 (2020).
14. K. L. Schulte et al., "Inverted metamorphic AlGaInAs/GaInAs tandem thermophotovoltaic cell designed for thermal energy grid storage application," *J. Appl. Phys.* **128**(14), 143103 (2020).
15. D. Chemisana, O. Teixidó, and R. Vaillon, "Silicon vertical multijunction cell for thermophotovoltaic conversion," *ACS Energy Lett.* **8**(8), 3520–3525 (2023).
16. R. M. Swanson, "Recent developments in thermophotovoltaic conversion," in *Int. Electron Devices Meeting*, IEEE, pp. 186–189 (1980).
17. E. J. Tervo et al., "Efficient and scalable GaInAs thermophotovoltaic devices," *Joule* **6**(11), 2566–2584 (2022).
18. B. Lee et al., "Air-bridge Si thermophotovoltaic cell with high photon utilization," *ACS Energy Lett.* **7**(7), 2388–2392 (2022).
19. R. Bhatt, I. Kravchenko, and M. Gupta, "High-efficiency solar thermophotovoltaic system using a nanostructure-based selective emitter," *Solar Energy* **197**, 538–545 (2020).
20. M. Shimizu, A. Kohiyama, and H. Yugami, "High-efficiency solar-thermophotovoltaic system equipped with a monolithic planar selective absorber/emitter," *J. Photonics Energy* **5**(1), 053099 (2015).
21. A. Kohiyama, M. Shimizu, and H. Yugami, "Unidirectional radiative heat transfer with a spectrally selective planar absorber/emitter for high-efficiency solar thermophotovoltaic systems," *Appl. Phys. Express* **9**(11), 112302 (2016).
22. L. Fraas et al., "TPV generators using the radiant tube burner configuration," in *Proc. 17th European PV Solar Energy Conf.*, Munich, Germany, Vol. **26** (2001).
23. Z. Omair et al., "Ultraefficient thermophotovoltaic power conversion by band-edge spectral filtering," *Proc. Natl. Acad. Sci. U. S. A.* **116**(31), 15356–15361 (2019).
24. C. Zhang et al., "A novel thermophotovoltaic optical cavity for improved irradiance uniformity and system performance," *Energy* **195**, 116962 (2020).
25. J. Fernández et al., "Back-surface optimization of Germanium TPV cells," *AIP Conf. Proc.* **890**(1), 190–197 (2007).
26. M. Suemitsu et al., "High-efficiency thermophotovoltaic system that employs an emitter based on a silicon rod-type photonic crystal," *ACS Photonics* **7**(1), 80–87 (2019).
27. T. Burger et al., "Semitransparent thermophotovoltaics for efficient utilization of moderate temperature thermal radiation," *Proc. Natl. Acad. Sci. U. S. A.* **119**(48), e2215977119 (2022).
28. J. Lim et al., "Enhanced photon utilization in single cavity mode air-bridge thermophotovoltaic cells," *ACS Energy Lett.* **8**, 2935–2939 (2023).
29. D. N. Woolf et al., "High-efficiency thermophotovoltaic energy conversion enabled by a metamaterial selective emitter," *Optica* **5**(2), 213–218 (2018).
30. A. Lenert et al., "A nanophotonic solar thermophotovoltaic device," *Nat. Nanotechnol.* **9**(2), 126–130 (2014).
31. M. W. Dashiell et al., "Quaternary InGaAsSb thermophotovoltaic diodes," *IEEE Trans. Electron Devices* **53**(12), 2879–2891 (2006).
32. Q. Lu et al., "Inas thermophotovoltaic cells with high quantum efficiency for waste heat recovery applications below 1000 c," *Solar Energy Mater. Solar Cells* **179**, 334–338 (2018).
33. R. Mittapally et al., "Near-field thermophotovoltaics for efficient heat to electricity conversion at high power density," *Nat. Commun.* **12**(1), 4364 (2021).
34. T. Inoue et al., "Integrated near-field thermophotovoltaic device overcoming blackbody limit," *ACS Photonics* **8**(8), 2466–2472 (2021).
35. T. Inoue et al., "One-chip near-field thermophotovoltaic device integrating a thin-film thermal emitter and photovoltaic cell," *Nano Lett.* **19**(6), 3948–3952 (2019).
36. J. Song et al., "Thermophotovoltaic energy conversion in far-to-near-field transition regime," *ACS Photonics* **9**(5), 1748–1756 (2022).
37. G. R. Bhatt et al., "Integrated near-field thermo-photovoltaics for heat recycling," *Nat. Commun.* **11**(1), 2545 (2020).
38. A. Fiorino et al., "Nanogap near-field thermophotovoltaics," *Nat. Nanotechnol.* **13**(9), 806–811 (2018).
39. C. Lucchesi et al., "Near-field thermophotovoltaic conversion with high electrical power density and cell efficiency above 14%," *Nano Lett.* **21**(11), 4524–4529 (2021).
40. M. A. Green, "Analytical treatment of Trivich–Flinn and Shockley–Queisser photovoltaic efficiency limits using polylogarithms," *Prog. Photovoltaics: Res. Appl.* **20**(2), 127–134 (2012).
41. J. Song et al., "Modeling and experiments of near-field thermophotovoltaic conversion: a review," *Solar Energy Mater. Solar Cells* **238**, 111556 (2022).

42. R. Mittapally et al., "Near-field thermophotovoltaic energy conversion: progress and opportunities," *Phys. Rev. Appl.* **19**(3), 037002 (2023).
43. E. López, I. Artacho, and A. Datas, "Thermophotovoltaic conversion efficiency measurement at high view factors," *Solar Energy Mater. Solar Cells* **250**, 112069 (2023).
44. K. Chen, P. Santhanam, and S. Fan, "Suppressing sub-bandgap phonon-polariton heat transfer in near-field thermophotovoltaic devices for waste heat recovery," *Appl. Phys. Lett.* **107**(9), 091106 (2015).
45. O. Dupré, R. Vaillon, and M. A. Green, "Physics of the temperature coefficients of solar cells," *Solar Energy Mater. Solar Cells* **140**, 92–100 (2015).
46. J. DeSutter, M. P. Bernardi, and M. Francoeur, "Determination of thermal emission spectra maximizing thermophotovoltaic performance using a genetic algorithm," *Energy Convers. Manage.* **108**, 429–438 (2016).
47. E. Blandre, R. Vaillon, and J. Drévillon, "New insights into the thermal behavior and management of thermophotovoltaic systems," *Opt. Express* **27**(25), 36340–36349 (2019).

Biographies of the authors are not available.